WHITE NOISE ANALYSIS OF *PHYCOMYCES* LIGHT GROWTH RESPONSE SYSTEM

II. EXTENDED INTENSITY RANGES

E. D. LIPSON

From the Division of Biology, California Institute of Technology, Pasadena, California 91125

ABSTRACT By means of white gaussian noise stimulation, the Wiener kernels are derived for the *Phycomyces* light growth response for a variety of intensity conditions. In one experiment the intensity I, rather than log I, is used as the input variable. Under the very limited dynamic range of that experiment, the response is fairly linear. To examine the dependence of the kernels on dynamic range, a series of experiments were performed in which the range of log I was halved and doubled relative to normal. The amplitude of the kernels, but not the time course, is affected strongly by the choice of dynamic range, and the dependence reveals large-scale nonlinearities not evident in the kernels themselves. In addition kernels are evaluated for experiments at a number of absolute intensity levels ranging from 10^{-12} to 10^{-3} W/cm^2. The kernel amplitudes are maximal at about 10^{-6} W/cm^2. At 10^{-12} W/cm^2, just above the absolute threshold, the response is very small. The falloff at high intensity, attributable to inactivation of the photoreceptor, is analyzed in the framework of a first-order pigment kinetics model, yielding estimates for the partial extinction coefficient for inactivation $\epsilon^I_{455} = (1.5 \pm 0.2) \times 10^4$ liter/mol · cm and a regeneration time constant of $\tau = (2.7 \pm 0.6)$ min. A model is introduced which associates the processes of adaptation and photoreceptor inactivation. The model predicts that the time constants for adaptation and pigment regeneration should be identical. This prediction is consistent with values in this and the preceding paper. The effects of pigment inactivation are simulated by a linear electronic analog circuit element, which may be cascaded with the linear simulator circuit in the preceding paper.

INTRODUCTION

In the preceding paper (Lipson, 1975; herein referred to as paper I), the Wiener-Lee-Schetzen formalism was employed for the practical identification of the functional of a nonlinear system. Although one may properly refer to *the* functional of such a system, the sequence of Wiener kernels obtained in a given experiment can provide only a partial representation of the system. This limitation applies over and above practical restrictions such as duration of the experiment, computed length of the kernels and truncation of the Wiener series. The fundamental problem is that in a given experiment one must preselect the dynamic range (defined below) and the operating

level of the gaussian white noise stimulus. Because the system is nonlinear, the kernels obtained will depend on these choices. In addition the kernels depend on values chosen for experimental parameters such as ambient temperature.

In paper I, the kernels were obtained under standard conditions defined therein. Here, the effects of various modifications of the stimulus parameters are investigated. The results shed light both on the system and on the white noise method itself. First the consequences of using light intensity $I(t)$, rather than log $I(t)$, for the white noise stimulus variable will be examined. Second, the dependence of the kernels on dynamic range of log $I(t)$ will be studied. Third, the dependence of the kernels on absolute intensity will be evaluated, by varying the log-mean intensity I_0 to span the whole visual range of *Phycomyces*. The results for the high intensity range will be examined in detail to help elucidate the inactivation and regeneration kinetics of the receptor pigment. Finally a model which associates adaptation directly with the photochemical kinetics will be presented and analyzed.

METHODS

The experimental procedures were similar to those in paper I with the following exceptions. For the experiment with *linear* modulation of light intensity the output voltage of the noise generator was fed directly to the intensity modulation input of the argon laser system.

To permit doubled dynamic range in one experiment, with randomization of log I, a second 4 OD circular neutral density wedge was added to the same shaft. Errors from multiple reflections were avoided by a slight tilt of the wedge axis relative to the laser beam. To reduce the dynamic range to half of normal, a single 4 OD wedge was used and the gain of the noise generator output was attenuated 50%.

Absolute intensity levels were set by means of neutral density filters and adjustment of the laser intensity. For experiments at the lowest intensity $I_0 = 10^{-12}$ W/cm^2, specimens were dark adapted for 30 min before the experiment. The first 45 min of the white noise data were excluded during analysis, to allow for adaptation to the white noise stimulus at the reference level I_0.

RESULTS

Linear Variation of Intensity

Except in this section, all kernels in this series of papers were obtained in terms of log $I(t)$ as input. The reasons for that choice were to achieve high dynamic range and to match an approximately logarithmic nonlinearity in the light growth response.

Here, for comparison, experiments were performed treating $I(t)$ itself as the input. In the identification experiments the gaussian white noise signal now was $I(t)$ rather than log $I(t)$. In a sense $I(t)$ is the "natural" input variable (measuring the flux of quanta incident on the receptor pigment), whereas the use of log $I(t)$ is rather artificial. However, it will be shown shortly how kernels for $I(t)$ may be derived from those for log $I(t)$ and vice versa. Thus, with some reservations the choice of input variable is arbitrary.

At this point it is worth clarifying the problem of dynamic range for this linear type

of experiment. The problem arises because the intensity, a *non-negative* variable, is required to have a *gaussian* distribution. In practice the gaussian distribution must be truncated, for example at three standard deviations ($\pm 3\ \sigma_I$) on each side of the mean $\bar{I}$. Now, define the "effective range" to be $\bar{I} \pm 2\ \sigma_I$, wherein the gaussian signal spends 95% of the time. In turn define the "dynamic range" to be the *ratio* of the limits of this effective range, i.e. $(\bar{I} + 2\ \sigma_I)/(\bar{I} - 2\ \sigma_I)$. In the present experiments the relation between $\bar{I}$ and σ_I was $\bar{I} = 3.5\ \sigma_I$. Thus, the dynamic range was 3.7:1. This is exceedingly low for a system like *Phycomyces* which can "see" over a range of orders of magnitude of intensity.

In contrast, variation of log $I(t)$ with a gaussian distribution places *no* limits on dynamic range of intensity. For the kernels presented in paper *I* the standard deviation of log I was $\sigma_L = 0.57$ decades. Thus the range $\pm 2\ \sigma_L$ about the log-mean intensity spans 2.28 decades or a dynamic range of 190:1 in intensity. In the following section kernels for other dynamic ranges will be presented.

In principle kernels for the alternative input variables $I(t)$ and log $I(t)$ can be deduced from one another as follows. Recall from paper I that the relative input and output variables $x(t) = \log_{10}(I(t)/I_0)$ and $y(t) = V(t) - V_0$ were employed, where V_0 was the mean velocity and I_0 was the "log-mean" intensity. With these relative variables, constant terms could be omitted and to second order:

$$y(t) = \int h_1(\tau)x(t - \tau)\mathrm{d}\tau + \int h_2(\tau_1,\tau_2)x(t - \tau_1)x(t - \tau_2)\mathrm{d}\tau_1\mathrm{d}\tau_2. \quad (1)$$

Here we similarly define the relative input $u(t) = I(t) - \bar{I}$ and obtain

$$y(t) = \int r_1(\tau)u(t - \tau)\mathrm{d}\tau + \int r_2(\tau_1,\tau_2)u(t - \tau_1)u(t - \tau_2)\mathrm{d}\tau_1\mathrm{d}\tau_2. \quad (2)$$

In both types of experiments the same reference intensity was used, i.e. $\bar{I} = I_0 = 1\ \mu\mathrm{W/cm^2}$. The relation between the two input variables then becomes

$$\begin{aligned} u &= I_0(10^x - 1) \\ &= aI_0x + a^2I_0x^2/2 + \ldots, \end{aligned} \quad (3)$$

where $a = \ln 10 = 2.303$. Substituting Eq. 3 into Eq. 2 and identifying terms to second order with Eq. 1, we obtain the relations

$$\begin{aligned} h_1(\tau) &= aI_0r_1(\tau), \\ h_2(\tau_1,\tau_2) &= a^2I_0^2r_2(\tau_1,\tau_2) + a^2I_0r_1(\tau_1)\delta(\tau_2 - \tau_1)/2, \end{aligned} \quad (4)$$

where $\delta(t)$ is the Dirac delta function. Conversely

$$\begin{aligned} r_1(\tau) &= h_1(\tau)/aI_0, \\ r_2(\tau_1,\tau_2) &= h_2(\tau_1,\tau_2)/a^2I_0^2 - h_1(\tau_1)\delta(\tau_2 - \tau_1)/2aI_0. \end{aligned} \quad (5)$$

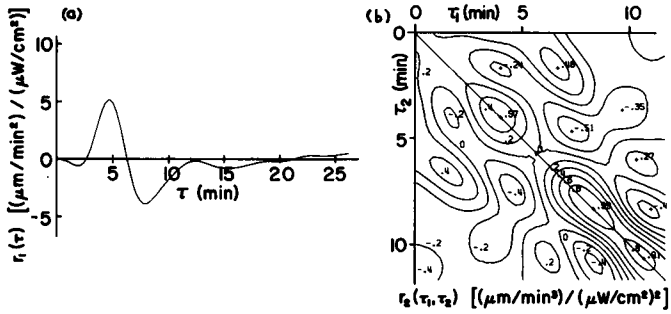

FIGURE 1 Kernels $r_1(\tau)$ and $r_2(\tau_1, \tau_2)$ obtained from experiments with white noise applied to the input variable $u(t) = I(t) - I_0$, which is linear with intensity.

Experimentally determined second order kernels r_2 and h_2 do not show mathematical singularities along the diagonal, implied by the delta function terms $\delta(\tau_2 - \tau_1)$. In practice this contribution is broadened by the limited bandwidths of the white noise stimulus and system response.

The kernels $r_1(\tau)$ and $r_2(\tau_1, \tau_2)$ are shown in Fig. 1. The kernels $h_1(\tau)$ and h_2 (τ_1, τ_2) were given in Fig. 2 of paper I. They are available below in this paper in Fig. 3 (with labels NDR to be explained later). As expected from Eq. 5, the shape of $r_1(\tau)$ is substantially the same as $h_1(\tau)$. Away from the diagonal region, the shape of r_2 is similar to that of h_2. The differences in structure along the diagonals of r_2 and h_2 largely fit the shape of h_1 (or r_1) as predicted by Eq. 5, in particular the splitting in r_2 of the long predominant diagonal peak of h_2.

A quantitative comparison of the magnitudes of h_1 and r_1 leads to an apparent discrepancy which will be resolved in the next section. Consider the magnitudes at the peak time $\tau_p = 5$ min. From Fig. 1*a*, $r_1(\tau_p) = 5.3$ $(\mu m/min^2)/(\mu W/cm^2)$. From Eq. 4 we would predict $h_1^{(pred)}(\tau_p) = 12.2$ $\mu m/min^2$. However from Fig. 3, $h_1(\tau_p) = 7.7$ $\mu m/min^2$. The source of the discrepancy is the great difference of dynamic range between the respective identification experiments. The experimental response shown in Fig. 2*b* is considerably smaller than that of Fig. 1*b* of paper I, thus illustrating the effect of lesser stimulus size. It will be explained in the next section how the dynamic range of the stimulus for a *nonlinear* system can so affect kernel magnitudes.

Another related point in Fig. 2 is the almost negligible contribution of r_2 (Fig. 2*e*) to the model response (Fig. 2*c*). This would seem to imply that the system is almost linear in terms of $I(t)$ as input. In paper I, the system seemed to be fairly linear with $\log I$ as input. Again the crucial factor of dynamic range must be invoked. Over the very small dynamic range of the present experiment, the (nonlinear) system behaves as if it were linear, whereas over the much larger dynamic range of the $\log I$ type experiment the system is better described as linear with $\log I$. Thus one must use caution in concluding from the present type of experiment with gaussian white noise applied linearly that a system is "linear," as the dynamic range over which the system is tested is rather shallow.

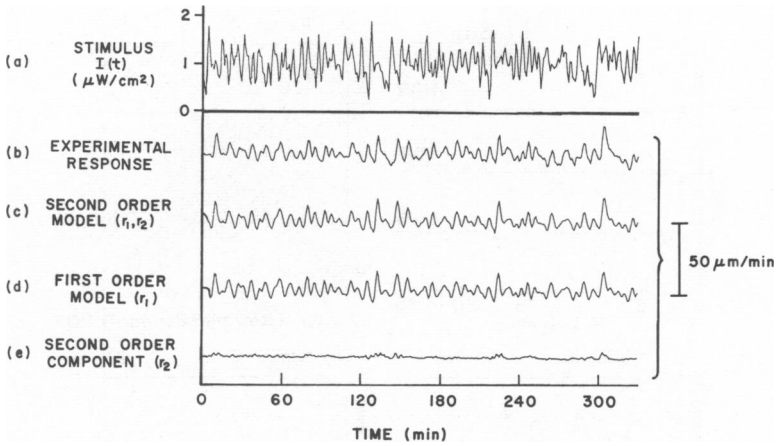

FIGURE 2 White noise stimulus (*a*), experimental response (*b*), and model responses (*c–e*) corresponding to the kernels of Fig. 1.

Dependence of Kernels on Dynamic Range

As mentioned above, the use of log I as the input permits unlimited flexibility with dynamic range. In this section results will be presented with the range of log $I(t)$ both doubled and halved relative to the standard experiment of paper *I*. In all experiments I_0 was 1 $\mu W/cm^2$. If the system were absolutely linear with log I, the kernels would be the same for all choices of dynamic range. Conversely, the dependence of the kernels on the choice of dynamic range can reveal large-scale nonlinear features beyond those exhibited by the nonlinear kernels themselves.

The respective kernels h_1 and h_2 are shown in Fig. 3. The shape of the kernels remains almost fixed while the amplitudes vary considerably. In the raw response data (not shown), the major positive and negative peaks of the response do not increase nearly in proportion to the stimulus range. This behavior may be viewed as a saturation of both extremes of the response. As the dynamic range increases, the saturation effect limits the kernel magnitudes. The adequacy of the kernels as measured by the mean-square error (MSE) criterion gets progressively worse as shown in Table I, particularly for the high range. As would be expected, the need for higher order kernels increases as the system is driven into this bilateral saturation. It should be emphasized, however, that even were higher order kernels to be computed, the dependence of the kernel of a given order, say h_1, upon dynamic range would persist because of the orthogonality of the Wiener series. The MSE data show that the normal dynamic range used throughout these papers is a good compromise between the opposing desires of maximizing dynamic range and minimizing the MSE for the second-order model.

The magnitude discrepancy of the last section between the first-order kernels $r_1(\tau)$ and $h_1(\tau)$ may now be viewed more clearly. The dynamic range of the "linear" experiment there was 3.7:1, even less than the low dynamic range experiment here. From the

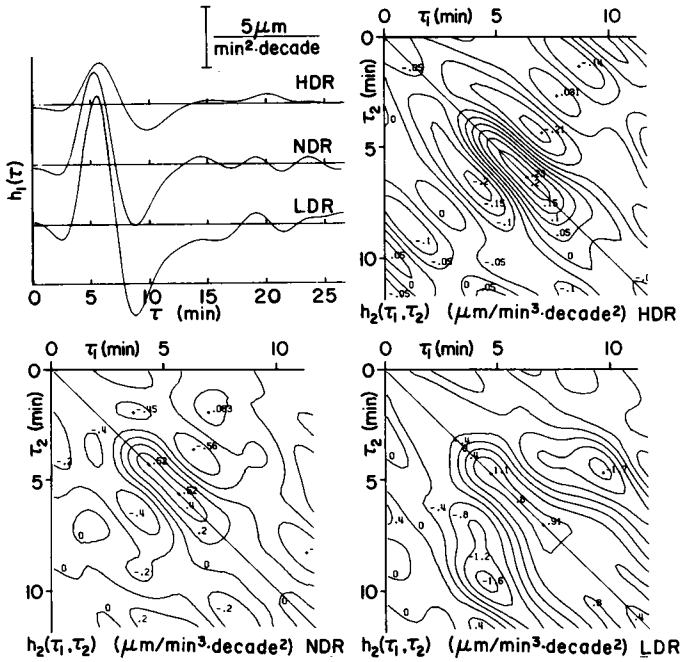

FIGURE 3 Kernels for high (HDR), normal (NDR) as in paper I, and low (LDR) dynamic ranges of the white noise stimulus, applied to $x(t) = \log_{10}(I(t)/I_0)$ with $I_0 = 10^{-6}$ W/cm^2. The values for dynamic range, as defined in the text, are given in Table I.

TABLE I

COMPARISON FOR KERNELS FOR DIFFERENT INTENSITY CONDITIONS

Kernels in Fig.	(Log-) mean intensity†	σ of gaussian noise	Dynamic range	No. of exp.	Mean velocity	MSE of model response*			Time of h_1 peak	Peak amplitude	
						Zero order	First order	Second order		h_1	h_2
	W/cm^2	*decades*			$\mu m/min$	$(\mu m/min)^2$	%	%	*min*	$\frac{\mu m/min^2}{decade}$	$\frac{\mu m/min^3}{decade^2}$
1	10^{-6}	0.28§	3.7:1	4	54	14	19.3	19.2	5.0	5.3‖	(1.)¶
3	10^{-6}	0.285	14:1	4	50	53	18.3	16.5	5.4	10.6	1.09
3, 5	10^{-6}	0.57	190:1	7	52	108	22.0	19.3	5.3	7.7	0.52
3	10^{-6}	1.14	36000:1	5	46	129	43.2	37.8	5.7	3.3	0.23
5	10^{-3}	0.57	190:1	4	66	3.5	59.4	51.2	5.1	1.1	−0.21
5	10^{-4}	0.57	190:1	3	60	21	19.3	15.3	5.0	3.8	(−0.2)
5	10^{-9}	0.57	190:1	3	47	49	39.5	35.6	6.6	3.8	0.59
5	10^{-12}	0.57	190:1	4	50	4.2	89.9	84.5	7.6	0.3	(0.1)

*Mean square errors between experimental and model response records. MSE for zero-order model (h_0) is in absolute units. MSEs for first-order (h_1) and second-order (h_1, h_2) models are given as percentages of zero-order MSE.

†Linear white noise in row 1; logarithmic noise in others. Row 3 is under standard conditions, as in paper I.

§In microwatts per square centimeter.

‖In (micrometers per minute^2)/(microwatts per centimeter^2).

¶In (micrometers per minute^3)/(microwatts per centimeter^2)^2.

values in Table I, one would expect an h_1 amplitude somewhat greater than 10.6 for the h_1 appropriate to that dynamic range, not inconsistent with the value of 12.2 deduced from $r_1(\tau)$. Thus the "discrepancy" is resolved. The foregoing underlines the importance of realizing the effects of dynamic range and making of a careful choice of it in white noise experiments.

Absolute Intensity Dependence

The kernels also depend on the reference intensity level I_0. The experiments described here were done under conditions similar to the standard experiment of paper I, except that a variety of I_0's was chosen to span the full intensity range over which *Phycomyces* can adapt. The kernels are shown in Fig. 4.

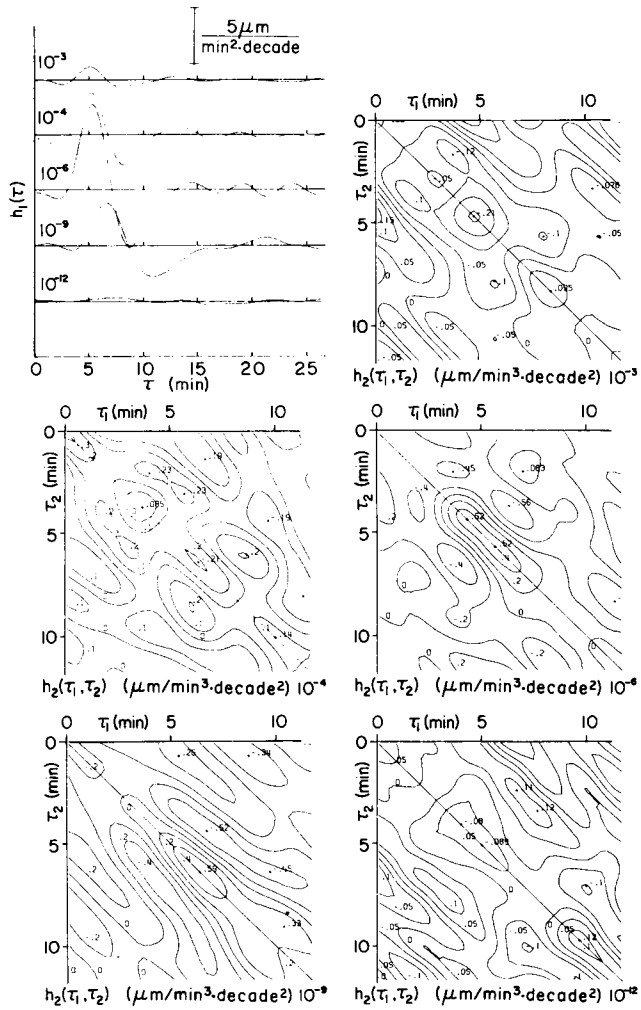

FIGURE 4 Kernels for different absolute intensity levels $I_0 = 10^{-3}$, 10^{-4}, 10^{-6}, 10^{-9}, and 10^{-12} W/cm^2.

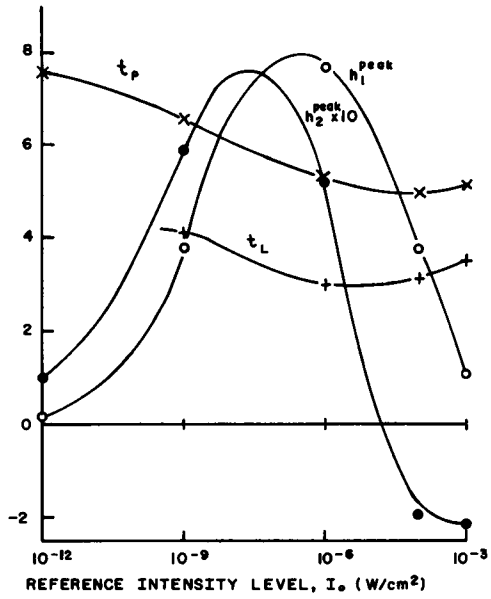

FIGURE 5

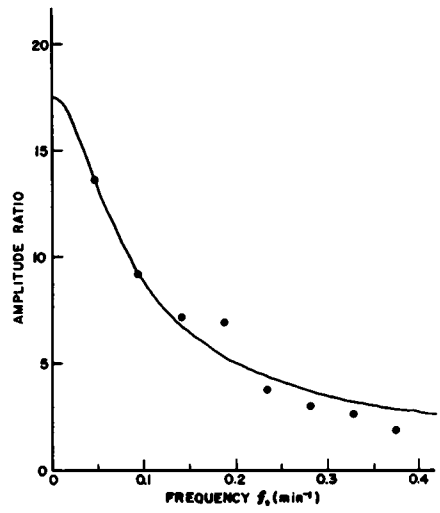

FIGURE 6

FIGURE 5 Absolute intensity dependence of latency (t_L), time of h_1 peak (t_P), and peak amplitudes of h_1 and h_2. The units on the ordinate are minutes for t_L and t_P; micrometers per minute^2 decade for h_1^{peak}; and micrometers per minute^3 decade^2 for $h_2^{peak} \times 10$.

FIGURE 6 Determination of pigment parameters by nonlinear least squares. The data points represent the ratio of the Fourier transform amplitudes for the first-order kernels at normal and high intensity. The curve represents the best fit to Eq. 24 with estimated parameters $f_1 = k/2\pi = (0.058 \pm 0.012)$ min^{-1} and $f_2 = cI_0/2\pi = (0.97 \pm 0.08)$ min^{-1}.

In Fig. 5 are plotted the absolute intensity dependence of the latency, peak time and peak amplitude of h_1, as well as of the peak amplitude of h_2. At the lower intensity levels the response becomes progressively delayed. The h_1 amplitude is maximal at about 10^{-6} W/cm^2, supporting this as a good choice for most experiments. At 10^{-9} W/cm^2 the h_1 amplitude has fallen 50% and by 10^{-12} W/cm^2 it has almost vanished. The sharp falloff at high intensity is interpreted in the next section in terms of a model for photoreceptor inactivation.

The h_2 amplitude curve in Fig. 5 is shifted toward lower intensity with a maximum at about 10^{-8} W/cm^2. In particular, the h_2 contribution is slightly greater at 10^{-9} W/cm^2 than at the standard 10^{-6} W/cm^2. At high intensity the h_2 peak becomes negative. Recall from paper I that the positive peak on the diagonal for normal (and now also for low) intensity was interpreted as rectification. The negative peak at high intensity may be interpreted similarly as *negative* rectification or, equivalently, as unipolar saturation on the positive side. In other words at high intensity a positive pulse stimulus should give a *smaller* response than a negative pulse.

Pigment Kinetics Model

The results at 10^{-3} W/cm^2 are of particular interest because of their potential in revealing the inactivation and regeneration kinetics of the receptor pigment. As yet the identity and location of the photoreceptor are unknown, although flavins are likely candidates. Information on the photochemical kinetics would offer an important assay for the pigment, particularly in relation to data on light-induced absorbance changes (Poff and Butler, 1974). In addition the pigment kinetics may play a key role in adaptation, as elaborated in the next section.

The differences between the kernels at 10^{-13} W/cm^2 and 10^{-6} W/cm^2 can be interpreted by the following simple model. Define p to be the fraction of active receptor pigment. Only in the high intensity range will p be appreciably less than unity. The number of quanta absorbed by active pigment is proportional to pI. If the response is normally some functional of $I(t)$, then at high intensity it should be the *same* functional of $p(t)I(t)$. Assume that the kinetics of p are governed by a first-order differential equation.

$$dp/dt = -cIp + k(1 - p), \tag{6}$$

where c is the cross section for inactivation and k is the regeneration rate constant. In the photostationary state, $p = 0.5$ for the "critical intensity" $I_c = k/c$. Thus the high intensity range may be defined as $I > I_c$.

The "monomolecular" photochemical equation 6 has been shown to describe well the bleaching and regeneration kinetics of cone pigments (Rushton, 1958) and rhodopsin (Alpern, 1971) in vertebrate vision, despite the known complexity of the photochemistry there.

The presumed inactivation of the *Phycomyces* photoreceptor complex might similarly be manifest as "bleaching," i.e. significant attenuation of peak(s) in the absorbance spectrum of the receptor pigment, producing a loss of (or change in) color. However, until positive spectroscopic data is available on the receptor pigment, it is advisable to use the more general term "inactivation."

The theoretical kernels for the above model are derived in the Appendix. Since the system was described well at 10^{-6} W/cm^2 and 10^{-3} W/cm^2 by first order kernels, the analysis here is restricted to first order. Eqs. 23 and 24 prescribe a fitting procedure for determining the model parameters k and c from the kernels at normal and high intensity. The results of the procedure are indicated in Fig. 6. From the frequency parameters f_1 and f_2 in the figure caption, one derives, respectively,

$$k = 2\pi f_1 = (0.37 \pm 0.08)\ \text{min}^{-1}$$

and

$$cI_0 = 2\pi f_2 = (6.1 \pm 0.5)\ \text{min}^{-1}.$$

The time constant of regeneration is

$$\tau = 1/k = (2.7 \pm 0.6)\ \text{min},$$

similar to the values of 7 min for vertebrate rhodopsin (Alpern, 1971) and 1–2 min for cone pigments (Rushton and Henry, 1968; Norren and Padmos, 1974).

Reexpressing $I_0 = 10^{-3}$ W/cm^2 (at $\lambda = 488$ nm) as $I_0 = 1.5 \times 10^{17}$ quanta/cm$^2 \cdot$ min, gives the inactivation cross section at 488 nm

$$c = (4.0 \pm 0.4) \times 10^{-17}\ \text{cm}^2.$$

The corresponding partial molar extinction coefficient for inactivation is

$$\epsilon^I_{488} = (1.1 \pm 0.1) \times 10^4\ \text{liter/mol} \cdot \text{cm}.$$

In the light growth response action spectrum Delbrück and Shropshire (1960), the sensitivity at 488 nm is about 70% of that at the peak wavelength of 455 nm. The partial extinction coefficient at the peak becomes

$$\epsilon^I_{455} = (1.5 \pm 0.2) \times 10^4\ \text{liter/mol} \cdot \text{cm}.$$

Finally, the critical intensity can be deduced from the ratio k/c as

$$I_c = (6 \pm 1) \times 10^{-5}\ \text{W/cm}^2$$

(at $\lambda = 488$ nm).

The value ϵ^I_{455} is comparable to the *total* extinction coefficient for vertebrate rhodopsin $\epsilon_{500} = 4 \times 10^4$ liter/mol $\cdot$ cm (Wald and Brown, 1953). Most biological pigments which have evolved for high sensitivity have their total extinction coefficient in this range, close to the theoretical limit for chromophores with broad absorption bands. The value ϵ^I_{455} provides a lower limit for the total extinction coefficient ϵ_{455} for the *Phycomyces* photoreceptor. Knowledge of the quantum yield for inactivation would reveal ϵ_{455} and vice versa. The large value of ϵ^I_{455} implies that the quantum yield for inactivation is not much below unity. The large quantum yield for inactivation suggests in turn that inactivation is "important" and may play a key role in the photochemistry of the light growth response.

A Model Identifying Adaptation with Pigment Kinetics

In vertebrate scotopic vision there does exist a clear relation between rhodopsin bleaching kinetics and dark adaptation (Rushton, 1965). Specifically, after strong bleaching, the fraction of unbleached rhodopsin and the *logarithm* of visual threshold follow similar exponential time courses in the dark with a time constant of about 7 min. Attempts to derive this relation from photochemical considerations alone have been generally unsuccessful, with the possible exception of a new model by Robinson (1975) involving

cooperativity of rhodopsin molecules in the disc membrane. Moreover, there are features of visual adaptation (Dowling, 1963) in addition to those related to photochemistry which indicate excitatory and inhibitory interactions between retinal cells. These features have been termed "neural adaptation."

In *Phycomyces,* which is a single cell, adaptation may be purely photochemical. If so, *Phycomyces* would serve as a clean model system for sensory adaptation at the molecular level. It is therefore of interest that the model for adaptation (Delbrück and Reichardt, 1956), analyzed in paper I, may be subsumed in the pigment kinetics model as follows. Assume first that the level of adaptation A is *solely* a function of p. In the photostationary state ($dp/dt = 0$, $dA/dt = 0$), $I = A$ and $p = (1 + cI/k)^{-1}$. Thus

$$p = (1 + cA/k)^{-1},$$
$$A = (k/c)\,[(1 - p)/p], \tag{7}$$

i.e., A is the critical intensity k/c times the ratio of inactive to active pigment. Now make the *ad hoc* (and simplest) assumption that this relation is true also in nonstationary situations. Substituting Eq. 7 into Eq. 6 then gives

$$dA/dt = k(I - A)(1 + cA/k). \tag{8}$$

In the normal intensity range where adaptation was studied (Delbrück and Reichardt, 1956), $A \ll k/c$ and Eq. 8 simplifies to

$$dA/dt \approx k(I - A), \tag{9}$$

which is identical to Eq. 8 of paper I *provided* the time constant of adaptation and the time constant of pigment regeneration are equal, $b = 1/k$. Recall the values $b = (4.2 \pm 1.5)$ min and $1/k = (2.7 \pm 0.6)$ min. The agreement within errors of these two values supports the proposed relationship between A and p. Adaptation experiments at high intensity would be valuable to check the validity of Eq. 8. Note that the correction term $(1 + cA/k)$ required at high intensity is simply $1/p$. Thus to a first approximation one would predict faster adaptation at high intensity (i.e., $b \rightarrow pb$).

According to the adaptation model (Delbrück and Reichardt, 1956) the response is a functional of I/A. From Eq. 7 we see that in the photostationary state this ratio takes on the form

$$I/A = cIp/k(1 - p). \tag{10}$$

The numerator and denominator are just the rate terms appearing on the right side of Eq. 6. Thus I/A appears more fundamentally as the ratio of the rates of inactivation and regeneration of the pigment. The question remains how such a *ratio* of rates could be computed by *Phycomyces.* The problem is simplified if one invokes logarithmic

transduction, whence

$$\log (I/A) = \log (cIp) - \log (k(1 - p)). \tag{11}$$

Then one needs only a *difference* amplifier.

Alternatively one can choose $(I - A)/A$ instead of I/A as the internal variable. This choice has the conceptual advantage of being zero in the adapted state. This ratio can be cast into the form (with the help of Eq. 6):

$$(I - A)/A = (1/k)(d/dt) \ln q, \tag{12}$$

where $q = 1 - p$ is the fraction of inactive pigment. It suggests that the response may be related directly to the amount of pigment in the inactive state. Eq. 12 suggests a cascade of logarithmic transducer acting on q and followed by a rate-sensitive (adaptive) element.

At the end of the next section the relationships 11 and 12 will be examined further, in the context of the adaptation simulator of paper I.

Electronic Simulation of Effects of Pigment Kinetics

The linear approximation of the pigment kinetics model introduces an element (see Appendix, Eq. 21) with the transfer function

$$P_1(s) = (s + k)/(s + k + cI_0) \tag{13}$$

corresponding to a first-order lead-lag filter (Milsum, 1966). This filter is represented by the electronic circuit of Fig. 7. By preceding the linear circuit of Fig. 6*a* in paper I with this variable pigment circuit, one extends the range of validity of the former to include the high intensity range.

In Fig. 8 are shown responses of the generalized linear simulator to pulses from various reference levels spanning the normal and high intensity ranges. At lower intensities the "pigment" element passes the input signal unchanged. Thus the response is the same as that of the normal-range simulator in paper I. At high intensity levels the circuit response amplitude becomes progressively diminished and the peaks and zero-crossings are shifted slightly to earlier times. The amplitude behavior agrees well with the kernels of Fig. 4 at 10^{-3}, 10^{-4}, and 10^{-6} W/cm^2. The delay (latency) of 2.5 min needed in paper I to align the circuit response with the kernel is not satisfactory at high intensity, particularly at $I_0 = 10^{-3}$ W/cm^2. The circuit response is faster, but the high intensity kernel is actually slower than that in the normal range. A latency of about 3.2 min is indicated from a comparison of the kernel and circuit response at $I_0 = 10^{-3}$ W/cm^2. This comparison magnifies the upturn of the latency curve at high intensity in Fig. 6. Note that in Fig. 6 latency was defined in terms of the kernel itself, whereas here we defined it as the shift of the circuit response needed to match the kernel.

Recall from paper I that the linear approximation of the adaptation model cor-

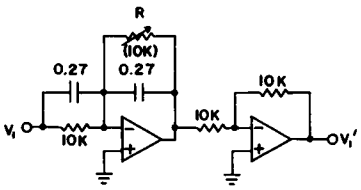

I (W/cm²)	R (kΩ)
10^{-3}	0.57
10^{-4}	3.8
10^{-5}	8.6
10^{-6}	9.8
10^{-7}	10.0

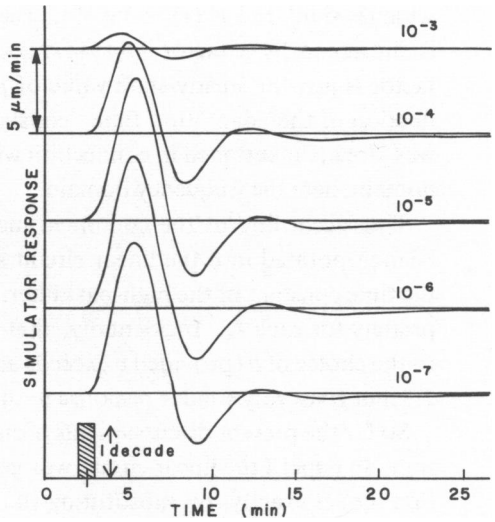

FIGURE 7

FIGURE 8

FIGURE 7 Electronic simulation of linear approximation (Eq. 13) of pigment kinetics model. The circuit consists of a lead-lag active filter followed by an inverter to restore the polarity. The reference intensity level I_0 is set by the variable resistor according to the formula $R(\text{k}\Omega) = 10/(1 + 16520 \cdot I_0)$, values for which are shown on the inset table. The input voltage V_1 and output voltage V_1' correspond respectively to the variables x and w (see Appendix), with conversion factors of 2 V:1 decade. Time has been scaled 1 ms:1 min. To simulate the small signal characteristics of the light growth response at any level I_0 in the normal and high intensity range, this circuit may be cascaded with the linear circuit of Fig. 6 *a* in paper I. Logically one would put the pigment first but, since linear elements commute, the order is arbitrary.

FIGURE 8 Output of combined linear simulator (Fig. 7 above, plus Fig. 6 *a* of paper I) in response to unit pulse (1 decade for 1 min) at various levels I_0 (W/cm^2). The units for amplitude and time have been converted to those appropriate to the experiments on *Phycomyces*. Since these curves are essentially unit impulse responses the amplitude scale here is numerically consistent with that of the first-order kernels in Fig. 4. A delay of 2.5 min (measured to the center of the pulse) has been included throughout to match the curve for 10^{-6} W/cm^2 to the corresponding kernel in Fig. 4.

responded to a high-pass filter with transfer function

$$F_1(s) = s/(s + 1/b). \tag{14}$$

The transfer function, $F_1'(s)$, for the cascade of $P_1(s)$ and $F_1(s)$ is

$$F_1'(s) = [s/(s + 1/b)] \cdot [(s + k)/(s + k + cI_0)]. \tag{15}$$

In the preceding section the model associating adaptation with pigment kinetics required $k = 1/b$. With this relation the cascade transfer-function simplifies to

$$F_1'(s) = s/(s + k + cI_0), \tag{16}$$

which is similar to $F_1(s)$ in Eq. 14, except that the adaptation time constant b (or $1/k$) is shortened by a factor $1/(1 + cI_0/k)$. According to the fundamental Eq. 7, this factor is just the steady-state value of p for the reference intensity level I_0. This reduction of the adaptation time "constant" by a factor p in the linear approximation was already mentioned in connection with Eq. 8 and 9. There the context was the time domain, here the frequency domain.

Thus according to the combined model, the effects of pigment inactivation could be incorporated into the linear circuit shown in Fig. 6 of paper I simply by adjusting the time constant of the high-pass filter, i.e. by reducing the feedback resistance appropriately for each I_0. Incidentally, that circuit for $I_0 = 10^{-6}$ W/cm^2 is very insensitive to the choice of b (provided b exceeds about 1 min). Specifically the choice $b = 1/k =$ 2.7 min gives very similar response to the nominal value $b = 4.2$ min.

So far the present discussion has been limited to the linear (small signal) approximation. In paper I the linear circuit was generalized to incorporate the nonlinear adaptation model exactly, by substituting the adaptation simulator (paper I, Fig. 8) for the high-pass filter. It is straightforward to design an analog circuit for the pigment kinetics model that serves as a generalization of the circuit in Fig. 7. The exact adaptation simulator would then be preceded by this exact pigment simulator. However in the spirit of the hypothesis of the preceding section associating these two phenomena, it is more instructive to modify the adaptation circuit to express directly the adaptation variable defined by Eq. 8.

A solution is given schematically in Fig. 9. The lower loop is similar to the original adaptation system (paper I, Fig. 8 *a*), except that in the feedback path z is divided by p before integration. The upper loop serves to compute $1/p$, given A from the, integrator output. At the bottom of the figure, signals corresponding to Eq. 11 and 12 are available. At normal intensity the present system reduces to the adaptation network of paper I.

This analog solution, while not unique in form, realizes the combined model for adaptation and pigment kinetics with a simple feedback network. Electronic implementation of the network of Fig. 9 is straightforward and will be helpful in testing the integrated model via adaptation experiments at high intensity. Moreover the scheme of Fig. 9 may suggest membrane and/or enzyme regulation mechanisms for pigment-mediated adaptation.

DISCUSSION

The problem of dynamic range is an important consideration for white noise experiments in general. In the special experiment with the input variable chosen as I rather than $\log I$, the dynamic range was unavoidably narrow. The finding that the system was approximately linear with I in this narrow range does not contradict the linearity of the system with $\log I$ over a larger range in paper I. Kernels from experiments with I or $\log I$ as input can be interrelated theoretically, so long as dynamic range is kept in mind. The first order kernels for both types of experiment are practically identical, as

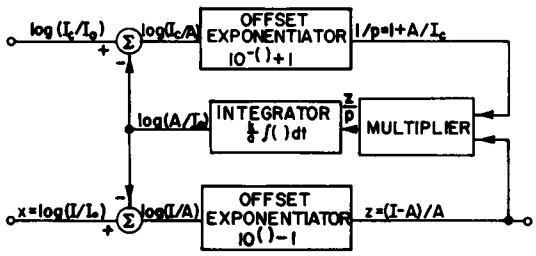

FIGURE 9

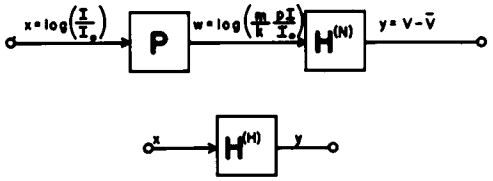

FIGURE 10

FIGURE 9 System representation of combined model for adaptation and pigment kinetics. Note that the input and output of the lower exponentiator can be expressed in terms of pigment variables according to Eq. 11 and Eq. 12.

FIGURE 10 Functional expression of pigment kinetics model. **P** is the pigment functional. $\mathbf{H}^{(N)}$ and $\mathbf{H}^{(H)}$ are the system functionals measured, respectively, at normal and high intensity.

expected. As a consequence, the input of the linear simulator circuit of Fig. 6*a* in paper I may be taken as $I(t)$, rather than $\log I(t)$, with suitable conversion of units and narrower restrictions on the range of validity. That range may be sufficient in particular for modeling phototropism in terms of the light growth response characteristics, as discussed in paper I.

Experiments were performed with the logarithmic range doubled and halved relative to the standard range of paper I. The general shape and time course of the kernels remain the same, but the kernel amplitudes diminish considerably as the dynamic range increases. For the high dynamic range the second-order Wiener model proves inadequate. These effects are attributable to a static nonlinearity, namely saturation of the response for large signals. This nonlinearity is probably associated with the growth control output in that there is a limit on the modulation amplitude of the growth velocity. The bipolar nature of this nonlinearity would require kernels of at least third order to describe it.

Unless one specifically desires to study this saturation nonlinearity, it is unprofitable to use dynamic range much beyond the standard range of paper I. It should be remembered that the enormous range of the light growth response is referred to the input not the output; the system can adapt gradually over about nine decades of light intensity, but at a given level the output becomes saturated by sudden changes of intensity over about two decades.

While a single white noise experiment could not span the entire visual range of *Phycomyces*, it is quite appropriate to perform separate experiments of limited range at a number of absolute operating levels. Thus the full range may be covered in steps. Kernels were presented for five such levels from $I_0 = 10^{-12}$ to 10^{-3} W/cm^2. The kernel amplitudes are maximal around $I_0 = 10^{-6}$ W/cm^2 which had been adopted as the normal range in these papers. The smallness of the kernels at $I_0 = 10^{-12}$ W/cm^2 reflected the absolute threshold of the system. The reduction of the kernel amplitudes at high intensity is interpretable by a simple model (Eq. 6) for inactivation and regen-

eration of the photoreceptor. Analysis of the model in the frequency domain led to estimates of $\tau = (2.7 \pm 0.6)$ min for the regeneration time constant and $\epsilon^{I}_{455} = (1.5 \pm 0.2) \times 10^4$ liter/mol · cm for the partial extinction coefficient for inactivation (i.e. the total extinction coefficient multiplied by the quantum yield for inactivation). Both of these values are comparable with corresponding parameters for human visual pigments (Alpern, 1971; Rushton and Henry, 1968).

These pigment parameters serve as a guide for spectrophotometric work aimed at identifying and localizing the photoreceptor by measuring light-induced absorbance changes (Poff and Butler, 1974; and unpublished work in this laboratory). So far the main assay for the photoreceptor has been the action spectrum, which suggests a flavin chromophore. The above parameters provide two further assay criteria. The closeness of the value of ϵ^{I}_{455} to the extinction coefficient of oxidized riboflavin ($\epsilon_{446} = 1.25 \times 10^4$ liter/mol · cm) supports the hypothesis that the photoreceptor is a flavin.

The phenomenon whereby the growth velocity becomes persistently elevated only in the high intensity range (Foster and Lipson, 1973) suggests a link between adaptation and the photopigment. At low and normal intensities, where only a negligible fraction of the photoreceptor is inactivated, the growth velocity adapts to any intensity level. The breakdown of this aspect of adaptation seems to coincide with the onset of appreciable inactivation. In general terms, the photochemistry of the receptor pigment would seem a logical context for the process of adaptation, both in the interests of simplicity (i.e. such that the photoreceptor controls its own sensitivity) and in order that adaptation be tied closely with the input of the sensory pathway. A model has been presented which relates the differential equation for adaptation to that for the pigment kinetics and relates the level of adaptation and the subjective intensity to the fraction of inactive pigment. The combined model may be tested further by adaptation and sunrise experiments in the high intensity range.

Just as a linear electronic circuit was presented in paper I to simulate the light growth response, here a circuit element was introduced to simulate the effects of pigment inactivation at high intensity. This circuit in cascade with that of paper I simulates the small scale behavior about *any* level in the normal or high intensity range. In paper I the circuit was adapted to allow for large scale (nonlinear) adaptation. Here it is shown how to modify that adaptation element further to include pigment kinetics in the context of the model that associates the two phenomena. The latter circuit will be helpful in designing and interpreting experimental tests of the combined model.

In terms of the role of *Phycomyces* as a model system for sensory processes at the cellular and molecular levels, the phenomenon of adaptation is of prime importance. *Phycomyces* adaptation has many correlates with vertebrate adaptation, including similarities in the kinetics and the absolute intensity range covered. But *Phycomyces* is much simpler, largely because of the absence of multicellular interactions. A prodigious amount of research on visual adaptation in animals has uncovered enormous complexity and sophistication. For example, while there appears to be a simple (although unexplained) relation between photoreceptor bleaching and the logarithm of visual threshold, adaptation appears to occur at the level of summation pools of

thousands of rods, rather than within the rods themselves (Rushton, 1965). It will continue to be difficult to unravel the fundamental processes and interactions. In particular the role of photochemical kinetics in adaptation is still in dispute. At the neural level, the roles of summation pools and lateral inhibition in adaptation are not understood satisfactorily.

Phycomyces demonstrates that rather similar adaptation can occur entirely within a single cell. In *Phycomyces,* adaptation is likely to involve photochemical kinetics and/or membrane processes. Elucidation of the mechanisms of adaptation in *Phycomyces* by methods of physiology, biochemistry, and genetics will be an important contribution to sensory biology and will probably offer new insights into the components of visual adaptation which reside in the receptor cells themselves.

APPENDIX

Kernels for Pigment Kinetics Model

For the pigment kinetics model presented in above, define a "pigment functional" **P** with input $x(t) = \log_{10}(I(t)/I_0)$ and output $w(t) = \log_{10}(mp(t)I(t)/cI_0)$ where $m = k + cI_0$. The kinetics of $p(t)$ are given by Eq. 6. Aside from the choice of logarithmic scale and normalization constants, **P** effectively transforms I into pI. The constants in the expression for w have been introduced so as to eliminate the zero-order kernel; i.e. so that $x(t) \equiv 0$ (photostationary state) implies $w(t) \equiv 0$, because $I(t) \equiv I_0$ gives $p(t) = p_0 \equiv k/m$.

In the framework of the model, the light growth response system may be decomposed functionally as shown in Fig. 10. The system functional $\mathbf{H}^{(H)}$ at high intensity (e.g. $I_0 = 10^{-3}$ W/cm^2) is equivalent to a cascade of the pigment functional **P** followed by the system functional $\mathbf{H}^{(N)}$, which is valid only at normal intensity (e.g. $I_0 = 10^{-6}$ W/cm^2). The functionals treated as operators (Barrett, 1963) are related by

$$\mathbf{H}^{(H)} = \mathbf{H}^{(N)} * \mathbf{P}. \tag{17}$$

$\mathbf{H}^{(H)}$ as shown in Fig. 9 is the general form. In the normal range ($I_0 \ll I_c = k/c$), when **P** becomes the identity operator, $\mathbf{H}^{(H)}$ reduces to $\mathbf{H}^{(N)}$.

Eq. 17 may be solved for **P** giving

$$\mathbf{P} = \mathbf{H}^{(N)-1} * \mathbf{H}^{(H)}. \tag{18}$$

Thus experimentally determined kernels for $\mathbf{H}^{(N)}$ and $\mathbf{H}^{(H)}$ may in principle be combined to deduce **P** or to test models (and evaluate parameters) for the kinetics of **P**. To examine the present model, it is necessary to evaluate the form of the kernels for **P** defined by

$$w(t) = \int p_1(\tau)x(t - \tau)\,d\tau + \int p_2(\tau_1, \tau_2)x(t - \tau_1)x(t - \tau_2)\,d\tau_1\,d\tau_2 + \cdots. \tag{19}$$

The differential Eq. 6 in terms of $I(t)$ and $p(t)$ may be reexpressed as one in terms of $x(t)$ and $w(t)$. The result, neglecting terms beyond second order in w and x, is

$$\dot{w} + mw - \dot{x} - kx + aw\dot{w} + ax\dot{x} - aw\dot{x} - ax\dot{w} + maw^2/2 + kax^2/2 - kawx = 0 \tag{20}$$

where the dots indicate time derivatives. By combining Eq. 19 with Eq. 20 one obtains two sets of differential equations involving only $p_1(t)$ and $p_2(t_1, t_2)$. Solving these with Laplace transforms one obtains

$$P_1(s) = (s + k)/(s + m),$$
$$P_2(s_1, s_2) = \frac{am(cI_0)^2}{2(s_1 + m)(s_2 + m)(s_1 + s_2 + m)} - \frac{acI_0}{2(s_1 + s_2 + m)}, \quad (21)$$

where $m \equiv k + cI_0$ and s is the Laplace transform variable.

According to Eq. 18 the relations between the kernels for $\mathbf{P}$, $\mathbf{H}^{(H)}$ and $\mathbf{H}^{(N)}$ are (Brilliant, 1958)

$$P_1(s) = H_1^{(H)}(s)/H_1^{(N)}(s),$$
$$P_2(s_1, s_2) = \frac{H_2^{(H)}(s_1, s_2)H_1^{(N)}(s_1 + s_2) - H_1^{(H)}(s_1 + s_2)H_2^{(N)}(s_1, s_2)}{H_1^{(N)}(s_1)H_1^{(N)}(s_2)H_1^{(N)}(s_1 + s_2)}, \quad (22)$$

where $H_1^{(H)}(s)$ is the Laplace transform of $h_1^{(H)}(t)$ and so on. Eq. 21 could in principle be fitted to these equations to evaluate k and c, as well as to judge the appropriateness of the model. However a rather complicated fitting procedure would be needed to fit jointly the first- and the second-order expressions. Recall though that the second-order kernels $h_2^{(N)}$ and $h_2^{(H)}$ contributed only slightly to the second-order model response. Therefore it seems suitable in the interests of simplicity and accuracy, to restrict the analysis to first order.

From Eq. 21 one can see that the magnitude of $P_1(s)$ increases with frequency, whereas the magnitude and relative accuracy of $H_1^{(H)}(s)$ and $H_1^{(N)}(s)$ fall off at high frequency. Thus it is statistically better to use the reciprocal $Q_1(s)$ of $P_1(s)$ in the fitting procedure. In the Pigment Kinetics Model section, the magnitude ratio of the transformed kernels $|H_1^{(N)}(s)| / |H_1^{(H)}(s)|$ is fit to the function $|Q_1(s)| = 1/|P_1(s)|$. Specifically, in terms of frequency $f = s/2\pi j$, the ratio

$$R(f) \equiv |H_1^{(N)}(2\pi jf)/H_1^{(H)}(2\pi jf)| \quad (23)$$

is fit to

$$Q_1(2\pi jf) = \left[\frac{f^2 + (f_1 + f_2)^2}{f^2 + f_1^2}\right]^{1/2} \quad (24)$$

where $f_1 = k/2\pi$ and $f_2 = cI_0/2\pi$.

I wish to thank Prof. Max Delbrück for encouragement and for criticism of the manuscript and Prof. Gilbert McCann for generously providing his computer facilities. I am indebted to Dr. Panos Marmarelis and Dr. Ken Foster for valuable discussions and to Messrs. Bruce Elgin, Dale Knutsen and Roque Szeto for assistance with computer software and hardware. I am grateful to Mr. Michael Walsh for excellent technical assistance and Mrs. Jeanette Navest for preparation of cultures.

This work was supported by grants from the National Science Foundation (BMS 70-00999 A04) and the National Institutes of Health (GM 21409) to Dr. M. Delbrück, and from the National Science Foundation (GJ 42025) and the National Institutes of Health (NS 03627) to Dr. G. D. McCann. The author held a postdoctoral fellowship (1 F02 GM 53785) from the National Institutes of Health.

Received for publication 18 February 1975.

REFERENCES

ALPERN, M. 1971. Rhodopsin kinetics in the human eye. *J. Physiol.* **217**:447.

BARRETT, J. F. 1963. The use of functionals in the analysis of nonlinear physical systems. *J. Electron. Control.* **15**:567.

BRILLIANT, M. B. 1958. Theory of the analysis of nonlinear systems. *Res. Lab. Electron. M.I.T. (Cambridge, Mass.) Tech. Rep.* 345.

DELBRÜCK, M., and W. REICHARDT. 1956. System analysis for the light growth reactions of *Phycomyces*. *In* Cellular Mechanisms in Differentiation and Growth. Dorothea Rudnick, editor. Princeton University Press, Princeton, N.J. 3–44.

DELBRÜCK, M., and W. SHROPSHIRE, JR. 1960. Action and transmission spectra of *Phycomyces*. *Plant Physiol.* **35**:194.

DOWLING, J. E. 1963. Neural and photochemical mechanisms of visual adaptation in the rat. *J. Gen. Physiol.* **46**:1287.

FOSTER, K. W., and E. D. LIPSON. 1973. The light growth response of *Phycomyces*. *J. Gen. Physiol.* **62**:590.

LIPSON, E. D. 1975*a*. White noise analysis of *Phycomyces* light growth response system. I. Normal intensity range. *Biophys. J.* **15**:989.

LIPSON, E. D. 1975*b*. White noise analysis of *Phycomyces* light growth response system. III. Photomutants. *Biophys. J.* **15**:1033.

MILSUM, J. H. 1966. Biological Control Systems Analysis. McGraw-Hill Book Company, New York.

NORREN, D. V., and P. PADMOS. 1974. Dark adaptation of separate cone systems studied with psychophysics and electroretinography. *Vis. Res.* **14**:677.

POFF, K. L., and W. L. BUTLER. 1974. Absorbance changes induced by blue light in *Phycomyces blakesleeanus* and *Dictyostelium discoideum*. *Nature (Lond.).* **248**:799.

ROBINSON, G. W. 1975. Rhodopsin cooperativity in visual response. *Vis. Res.* **15**:35.

RUSHTON, W. A. H. 1958. Kinetics of cone pigments measured objectively on the living human fovea. *Ann. N.Y. Acad. Sci.* **74**:291.

RUSHTON, W. A. H. 1965. Visual adaptation. *Proc. R. Soc. Lond. B Biol. Sci.* **162**:20.

RUSHTON, W. A. H., and G. H. HENRY. 1968. Bleaching and regeneration of cone pigments in man. *Vis. Res.* **8**:617.

WALD, G., and P. K. BROWN. 1953. The molecular extinction of rhodopsin. *J. Gen. Physiol.* **37**:189.